Monthly Notices
of the
ROYAL ASTRONOMICAL SOCIETY

Mon. Not. R. Astron. Soc. **423,** 2680–2689 (2012) doi:10.1111/j.1365-2966.2012.21075.x

The density variance–Mach number relation in supersonic turbulence – I. Isothermal, magnetized gas

F. Z. Molina,[1]★† S. C. O. Glover,[1] C. Federrath[1,2,3] and R. S. Klessen[1]

[1]*Institut für Theoretische Astrophysik, Zentrum für Astronomie der Universität Heidelberg, Albert-Ueberle-Str. 2, 69120 Heidelberg, Germany*
[2]*Ecole Normale Supérieure de Lyon, Centre de Recherche Astrophysique, 46 Allée d'Italie, F-69364 Lyon, France*
[3]*Monash Centre for Astrophysics (MoCA) and School of Mathematical Sciences, University of Monash, VIC 3800, Australia*

Accepted 2012 April 5. Received 2012 April 5; in original form 2011 November 7

ABSTRACT

It is widely accepted that supersonic, magnetized turbulence plays a fundamental role for star formation in molecular clouds. It produces the initial dense gas seeds out of which new stars can form. However, the exact relation between gas compression, turbulent Mach number and magnetic field strength is still poorly understood. Here, we introduce and test an analytical prediction for the relation between the density variance and the rms Mach number $\mathscr{M}$ in supersonic, isothermal, magnetized turbulent flows. We approximate the density and velocity structure of the interstellar medium as a superposition of shock waves. We obtain the density contrast considering the momentum equation for a single magnetized shock and extrapolate this result to the entire cloud. Depending on the field geometry, we then make three different assumptions based on observational and theoretical constraints: B independent of ρ, $B \propto \rho^{1/2}$ and $B \propto \rho$. We test the analytically derived density variance–Mach number relation with numerical simulations, and find that for $B \propto \rho^{1/2}$, the variance in the logarithmic density contrast, $\sigma^2_{\ln \rho/\rho_0} = \ln[1 + b^2\mathscr{M}^2\beta_0/(\beta_0 + 1)]$, fits very well to simulated data with turbulent forcing parameter $b = 0.4$, when the gas is super-Alfvénic. However, this result breaks down when the turbulence becomes trans-Alfvénic or sub-Alfvénic, because in this regime the turbulence becomes highly anisotropic. Our density variance–Mach number relations simplify to the purely hydrodynamic relation as the ratio of thermal to magnetic pressure $\beta_0 \to \infty$.

Key words: MHD – shock waves – turbulence – stars: formation – ISM: clouds – ISM: magnetic fields.

1 INTRODUCTION

Detailed knowledge about the statistical characteristics of the density structure is of pivotal importance for many fields in astronomy and astrophysics. Probability distribution functions (PDFs) of the density have been introduced as a simple and robust measure of the one-point statistics for many applications, ranging from cosmology, where the Press–Schechter formalism was primarily established (Press & Schechter 1974), to star formation and theories of the initial mass function or the core mass function (e.g. Fleck 1982; Zinnecker 1984; Padoan, Nordlund & Jones 1997; Klessen & Burkert 2000; Li et al. 2004; Hennebelle & Chabrier 2008, 2009; Padoan & Nordlund 2011).

In the star formation context, the relation between the width of the density PDF – the density variance or standard deviation – and the rms Mach number in supersonic turbulent flow is a key ingredient for analytical models of the star formation rate (Krumholz & McKee 2005; Padoan & Nordlund 2011) and for the stellar initial mass function or the core mass function (Padoan & Nordlund 2002; Hennebelle & Chabrier 2008, 2009). In this framework, supersonic turbulence plays a fundamental role in determining the density and velocity statistics of the interstellar medium (Elmegreen & Scalo 2004; McKee & Ostriker 2007) and controls stellar birth (Mac Low & Klessen 2004). Conversely, the importance of magnetic fields in the star formation process is still inconclusive, despite decades of research (Mouschovias & Ciolek 1999; McKee & Ostriker 2007; Crutcher, Hakobian & Troland 2009; Crutcher et al. 2010; Bertram et al. 2012). Hence, the question of how magnetic fields affect the density variance–Mach number relation is still not clearly answered, despite the empirical findings of Ostriker, Stone & Gammie (2001) and the analytical ansatz provided by Padoan & Nordlund (2011).

For purely hydrodynamical, supersonic, isothermal, turbulent gas, the relation between the density variance and Mach number

★Member of the International Max Planck Research School for Astronomy and Cosmic Physics at the University of Heidelberg (IMPRS-HD) and the Heidelberg Graduate School of Fundamental Physics (HGSFP).
†E-mail: molina@stud.uni-heidelberg.de

has been identified and widely studied in numerical simulations (e.g. Padoan et al. 1997; Passot & Vázquez-Semadeni 1998; Federrath, Klessen & Schmidt 2008b; Federrath et al. 2008a, 2010; Price, Federrath & Brunt 2011). This relation is commonly assumed to be linear:

$$\sigma_{\rho/\rho_0} = b\mathscr{M}, \tag{1}$$

where σ^2_{ρ/ρ_0} is the density variance (to emphasize the density fluctuations about the mean ρ_0, it makes sense to express the density in terms of the density contrast ρ/ρ_0), b is a proportionality constant of order unity as explained in more detail below and $\mathscr{M}$ is the rms Mach number. Usually, the density contrast is written in terms of its logarithm, $s \equiv \ln(\rho/\rho_0)$.

Several authors have noted that the PDF of the logarithm of the density contrast s – produced by supersonic turbulent flow of isothermal gas – follows approximately a lognormal distribution (e.g. Vázquez-Semadeni 1994; Padoan et al. 1997; Passot & Vázquez-Semadeni 1998; Nordlund & Padoan 1999; Klessen 2000; Ostriker et al. 2001; Li, Klessen & Mac Low 2003; Kritsuk et al. 2007; Federrath et al. 2008b; Lemaster & Stone 2008; Schmidt et al. 2009; Federrath et al. 2010; Glover et al. 2010; Collins et al. 2011; Padoan & Nordlund 2011; Price et al. 2011),

$$p_s \mathrm{d}s = \frac{1}{\sqrt{2\pi\sigma_s^2}} \exp\left[-\frac{(s-s_0)^2}{2\sigma_s^2}\right] \mathrm{d}s, \tag{2}$$

where the mean s_0 is related to the density variance by $s_0 = -\sigma_s^2/2$, due to the constraint of mass conservation. Besides the empirical findings of Vázquez-Semadeni (1994), Padoan et al. (1997) and Passot & Vázquez-Semadeni (1998), there is no clear explanation for the shape of the PDF. From a mathematical point of view, a lognormal distribution is the result of independent random perturbations driven in a stationary system (Pope & Ching 1993) as a consequence of the central limit theorem (Vázquez-Semadeni 1994; Padoan et al. 1997; Nordlund & Padoan 1999; Federrath et al. 2010). The physical interpretation is that density fluctuations present at a given location are produced by successive passages of shocks with amplitudes independent of the local density. For a lognormal distribution, the density variance – given by equation (1) – is equivalent to

$$\sigma_s^2 = \ln\left[1 + b^2\mathscr{M}^2\right]. \tag{3}$$

The parameter b in equations (1) and (3) is related to the kinetic energy injection mechanism – the forcing $\boldsymbol{F}$, which drives the turbulence. Federrath et al. (2008b) found that $b = 1$ for purely compressive (curl-free) forcing, $\nabla \times \boldsymbol{F} = 0$, while $b = 1/3$ for purely solenoidal (divergence-free) forcing, $\nabla \cdot \boldsymbol{F} = 0$. In a follow-up study, Federrath et al. (2010) showed that b increases smoothly from 1/3 to 1, when the amount of compressive modes, $F_{\rm comp}/(F_{\rm sol} + F_{\rm comp})$, is gradually increased from 0 to 1. For the natural mixture of modes, $F_{\rm comp}/(F_{\rm sol} + F_{\rm comp}) = 1/3$, which is also the mixture of forcing modes used in all our numerical experiments here, they found $b \approx 0.4$, so we will later use that value for comparing our analytic model with numerical simulations.

When magnetic fields are included, the density variance is significantly lower than in the unmagnetized case for simulations with Mach numbers $\mathscr{M} \gtrsim 10$ (Ostriker et al. 2001; Price et al. 2011). Recently, Padoan & Nordlund (2011) provided an analytical ansatz for the hydrodynamical density contrast in supersonic, turbulent flow, which in turn follows the approach of Dyson & Williams (1980) for obtaining the density contrast for strong adiabatic shocks, but extended to the magnetic case. Their σ_s–$\mathscr{M}$ relation was, however, not tested with numerical simulations.

The density PDF may or may not deviate from a lognormal form when other processes – like heat exchange and gravitation – are included. For example, when a non-isothermal equation of state is considered, the PDF still closely follows a lognormal distribution over a range of densities (see e.g. Glover & Mac Low 2007). However, depending on whether the equation of state is softer or harder than isothermal, it might acquire power-law tails at either high or low densities (Passot & Vázquez-Semadeni 1998; Scalo et al. 1998; Wada 2001; Li et al. 2003; McKee & Ostriker 2007). The density PDF also deviates from lognormal when gravity is included. In this instance, the PDF exhibits a power-law tail at high densities (Klessen 2000; Federrath et al. 2008a; Kainulainen et al. 2009; Cho & Kim 2011; Kritsuk, Norman & Wagner 2011). In addition, turbulent intermittency also leads to deviations from the lognormal PDF in the wings of the distribution (Federrath et al. 2010). Consequently, the accuracy of the measurement of the density variance, using equation (2), may be compromised depending on the importance of the different processes involved in real molecular clouds.

Here, we present an analytical derivation for the σ_s–$\mathscr{M}$ relation in supersonic turbulent isothermal gas including magnetic fields. Our results are in qualitative agreement with Ostriker et al. (2001) and Price et al. (2011); however, here we present quantitative predictions and tests. The present work is organized as follows. In Section 2 we describe the analytical approach made for the σ_s–$\mathscr{M}$ relation. In this section, we start with the study of the density contrast of a single shock confined into a cubic box, and then we extrapolate it to the whole cloud in Section 2.1. In Section 2.2 we propose three σ_s–$\mathscr{M}$ relations given by three different assumptions of the behaviour of magnetic fields with density. We test these predictions with numerical simulations in Section 3 and conclude in Section 4.

2 ANALYTICAL DERIVATION

Our basis for obtaining the density variance–Mach number relationship involves determining how the density contrast changes with the Mach number. The density variance σ_{ρ/ρ_0} and the density contrast are related by

$$\sigma^2_{\rho/\rho_0} = \frac{1}{V}\int_V \left(\frac{\rho}{\rho_0} - 1\right)^2 \mathrm{d}V, \tag{4}$$

where ρ is the local density, ρ_0 is the mean density in the volume and V is the volume of the cloud. The density contrast is a measure of the density fluctuations in the flow, and therefore it is useful for identifying the disturbances that originate from shock fronts and compressions.

2.1 Density contrast in magnetohydrodynamics

Supersonic turbulence in the interstellar medium generates a complex network of shock waves (or simply shocks). When the velocity of the fluid exceeds that of sound, it leads to the formation of shocks that are one of the most important distinctive effects of the compressibility of the fluid (e.g. Landau & Lifshitz 1987).

In order to study the density contrast in a molecular cloud, we first consider the physics of the discontinuity formed by a single shock front. We then generalize the results to the ensemble of shocks confined in a cloud. Following Lequeux (2005), we describe a shock by choosing two control surfaces, one on either side of the discontinuity and parallel to each other. Let us choose the shock surfaces as the reference frame, such that the control surfaces are stationary with respect to the shock. We also define the 'parallel' direction

as the one parallel to the flow of gas through the shock (i.e. perpendicular to the shock front). From the well-known equations of fluid dynamics, it is then possible to derive equations that express the conservation of matter and momentum flux for a magnetized inviscid, neutral fluid,

$$v_{\parallel,1}\rho_1 = v_{\parallel,2}\rho_2 \tag{5}$$

and

$$\rho_1\left(v_{\parallel,1}^2 + \frac{c_{\mathrm{s},1}^2}{\gamma_1} + \frac{v_{\mathrm{A}\perp,1}^2}{2}\right) = \rho_2\left(v_{\parallel,2}^2 + \frac{c_{\mathrm{s},2}^2}{\gamma_2} + \frac{v_{\mathrm{A}\perp,2}^2}{2}\right), \tag{6}$$

respectively. In these equations, the subscripts 1 and 2 indicate the pre- and post-shock conditions, respectively. The velocity of the gas into the shock is $v_\parallel$, while c_s is the adiabatic sound speed, γ is the ratio between the specific heats and $v_{\mathrm{A}\perp}$ is the Alfvén velocity, defined here as $v_{\mathrm{A}\perp} = B_\perp/(4\pi\rho)^{1/2}$, where $B_\perp$ is the magnetic field perpendicular to the flow direction. The post-shock density is described by ρ_2.

We now make two important approximations. First, as we wish to focus on the role of magnetic fields in determining the density variance, we assume that the gas is isothermal, deferring consideration of non-isothermal effects to future work. Our assumption of isothermality implies that $c_{\mathrm{s},1} = c_{\mathrm{s},2} = c_\mathrm{s}$ and $\gamma_1 = \gamma_2 = 1$. Secondly, as we are considering an entire molecular cloud, we approximate it as an ensemble of shocks. We assume that we can express the average pre-shock velocity in terms of the rms velocity v_0 – hereafter, the subscript '0' indicates the volume averages – as $v_{\parallel,0}^2 = b^2 v_0^2$, where the factor b depends on the number of degrees of freedom available for the compressive modes (Federrath et al. 2008b). We also assume that the typical pre-shock magnetic and thermal pressures are just those given by volume averages over the total volume, allowing us to write them in terms of the volume-averaged density ρ_0 and the rms Alfvénic velocity $v_{\mathrm{A},0}$. Similarly, we assume that the typical pre-shock density is simply the volume-averaged density. Making these assumptions, and introducing the ratio of the thermal pressure to magnetic pressure

$$\beta \equiv \frac{P_\mathrm{th}}{P_\mathrm{mag}} = 2\frac{c_\mathrm{s}^2}{v_\mathrm{A}^2}, \tag{7}$$

we can rewrite equation (6) as

$$b^2\mathscr{M}^2\frac{\rho_0}{\rho_2}\left(1 - \frac{\rho_0}{\rho_2}\right) + \frac{\rho_0}{\rho_2}\left(1 + \beta_0^{-1}\right) = \left(1 + \beta_2^{-1}\right), \tag{8}$$

where the rms Mach number is given by $\mathscr{M} = v_0/c_\mathrm{s}$.

In order to solve this equation for the characteristic density contrast associated with the shocked gas, ρ_2/ρ_0, it is necessary to determine β_2, the post-shock ratio of the thermal to magnetic pressures. The value of this will depend on the change in the magnetic field strength through the shock, which in turn depends on the orientation of the field with respect to the flow of gas through the shock. Using magnetic flux and mass conservation during compression, one can show that $B \propto \rho^\alpha$, with $0 \leq \alpha \leq 1$, depending on the field geometry and direction of compression. In the extreme case where the gas flows in a direction parallel to the field lines, the field strength will be the same on either side of the shock despite the jump in density, and the field strength then will be independent of density, i.e. $\alpha = 0$. In the other extreme case where the field is oriented at right angles to the gas flow, the shock jump conditions for magnetic flux freezing imply that $B \propto \rho$, i.e. $\alpha = 1$. Meanwhile, compression of an isotropic field along all three spatial directions gives $B \propto \rho^{2/3}$. However, for our 'average shock', we expect a behaviour that lies somewhere between $0 \lesssim \alpha \lesssim 1$. By looking at observations and existing simulations, we can get some guidance as to what this intermediate behaviour should be.

Observationally, Crutcher (1999) presented a study of the magnetic field strength in molecular clouds measured with the Zeeman effect. He fitted the results with a power law $B \propto \rho^\alpha$ and found that $\alpha = 0.47 \pm 0.08$. Crutcher, Heiles & Troland (2003) provided additional support for this result. More recently, Crutcher et al. (2010) have presented a detailed compilation of Zeeman data based on a much larger number of measurements. They find that at number densities $n < 300\,\mathrm{cm}^{-3}$, the data are consistent with a field strength that is independent of density, while at higher densities they obtain $B \propto \rho^{0.65\,\pm0.05}$.

From a theoretical point of view, Padoan & Nordlund (1999) noted that their B distributions closely match the observational scaling given by Crutcher (1999) and Crutcher et al. (2003), $B \propto \rho^{1/2}$, for high B in their high Alfvénic Mach number regime. Kim, Balsara & Mac Low (2001) also study the relationship between B and ρ, and find that $\alpha \simeq 0.4$, albeit with large scatter, especially at low densities. Additionally, Banerjee et al. (2009) report that the magnetic field strength appears to scale in their simulations as $B \propto \rho^{1/2}$ for number densities $10^2 \lesssim n \lesssim 10^4\,\mathrm{cm}^{-3}$, although with significant scatter around this value. On the other hand, Hennebelle & Pérault (2000) found that the magnetic field does not necessarily increase with the density. Aside from these reports, if the magnetic flux is not conserved, but increases due to turbulent dynamo amplification during compression, α can become larger than the values quoted above, depending on the Reynolds numbers of the gas (Schleicher et al. 2010; Sur et al. 2010; Federrath et al. 2011). Thus, even if the gas is compressed only parallel to the field lines, turbulent tangling of the field can lead to $\alpha > 0$ during compression.

Given the different possible relations between the magnetic field strength and the density, we consider three cases to include in equation (8): the two extreme cases, where B is independent of the density and where $B \propto \rho$, and an intermediate case with $B \propto \rho^{1/2}$. We also note that if we were to take instead the relation $B \propto \rho^{0.65}$ suggested by the most recent observational data, then we would obtain results quite similar to the $B \propto \rho^{1/2}$ case.

2.1.1 *First case: B independent of ρ*

We start by considering one extreme, the case where B is independent of the density. In this scenario, equation (8) becomes a second-order equation, independent of the magnetic field strength

$$\left(\frac{\rho_2}{\rho_0}\right)^2 - \left(b^2\mathscr{M}^2 + 1\right)\left(\frac{\rho_2}{\rho_0}\right) + b^2\mathscr{M}^2 = 0.$$

This equation results in a density contrast

$$\frac{\rho_2}{\rho_0} = b^2\mathscr{M}^2. \tag{9}$$

Equation (9) matches the density contrast for the non-magnetic regime (see e.g. Padoan et al. 1997). This is not surprising, because in this case we are assuming that the gas and the magnetic field are not coupled. Therefore, amplification of the magnetic field with density is not expected under these conditions.

2.1.2 *Second case: B ∝ ρ^1/2*

In the intermediate case in which $B \propto \rho^{1/2}$, we again find a second-order equation for the density contrast, but with a dependence on

the magnetic field expressed in terms of β_0. From equation (8), we obtain

$$\left(1+\beta_0^{-1}\right)\left(\frac{\rho_2}{\rho_0}\right)^2-\left(b^2\mathscr{M}^2+1+\beta_0^{-1}\right)\left(\frac{\rho_2}{\rho_0}\right)+b^2\mathscr{M}^2=0.$$

This equation has the solution

$$\frac{\rho_2}{\rho_0}=b^2\mathscr{M}^2\left(\frac{\beta_0}{\beta_0+1}\right). \tag{10}$$

In other words, the effect of the magnetic field in this case is to reduce the density contrast by a factor $\beta_0/(\beta_0+1)$. We see from this that in the weak field limit where $\beta_0\to\infty$, we recover the hydrodynamical result, while for strong fields we have a smaller density contrast in the magnetohydrodynamic (MHD) case than in the non-magnetic case.

2.1.3 *Third case: $B\propto\rho$*

Finally, we investigate the other extreme case, where the magnetic field strength is proportional to the density. In this case, equation (8) results in a third-order equation,

$$\beta_0^{-1}\left(\frac{\rho_2}{\rho_0}\right)^3+\left(\frac{\rho_2}{\rho_0}\right)^2-\left(b^2\mathscr{M}^2+1+\beta_0^{-1}\right)\left(\frac{\rho_2}{\rho_0}\right)+b^2\mathscr{M}^2=0.$$

The solution for the density contrast is

$$\frac{\rho_2}{\rho_0}=\frac{1}{2}\left(-1-\beta_0+\sqrt{(1+\beta_0)^2+4b^2\mathscr{M}^2\beta_0}\right). \tag{11}$$

2.2 Density variance–Mach number relation

In the previous section, we presented three different expressions for the density contrast. They correspond to three different assumptions regarding the relationship $B\propto\rho^\alpha$, with $\alpha=0$, 1/2 and 1. We now determine the density variance of a fluid in which there are many shocks, for each of these three cases.

We start by noting that in a highly supersonic flow, the dominant contribution to the integral in equation (4) will come from shocked regions, and thus we can consider this equation as a volume average over an ensemble of many shocks. We next assume that we can approximate the value of this integral with the result of integrating over a single 'average' shock of the kind considered in the previous section. As we already know the density contrast of this representative shock, the only thing that remains to be done before we can solve equation (4), is to determine the appropriate volume over which to integrate.

We approximate the cloud as a cubic box of side L, and consider an infinitesimal part of its volume $\mathrm{d}V$ that encloses one shock. Therefore, the size of $\mathrm{d}V$ depends on the size of the shock itself:

$$\mathrm{d}V\approx\mathrm{d}V_{\rm sh}. \tag{12}$$

To define the shock volume, we make use of an approximation introduced by Padoan & Nordlund (2011), where the volume of the shock is given by the area of the box face times the shock width λ, $V_{\rm sh}=L^2\lambda$. However, in the absence of viscosity, it is not straightforward to define the shock width λ. Therefore, we follow Padoan & Nordlund (2011) and assume that the shock width, if the compression is driven at the box scale, is given by

$$\lambda\simeq\theta L\rho_0/\rho_2, \tag{13}$$

where θ is the integral scale of the turbulence. Then, the volume of the shock $V_{\rm sh}$ is given by

$$V_{\rm sh}\simeq\theta L^3\frac{\rho_0}{\rho_2}. \tag{14}$$

For turbulence driven on large scales, as appears to be the case in real molecular clouds (Ossenkopf & Mac Low 2002; Brunt, Heyer & Mac Low 2009), we have $\theta\simeq1$. Having made the assumption that the appropriate volume over which to average is the volume of our representative shock, and considering equation (15), we approximate $\mathrm{d}V$ by

$$\mathrm{d}V=L^3\left(\frac{\rho_0}{\rho_2}\right)^2\mathrm{d}\left(\frac{\rho_2}{\rho_0}\right). \tag{15}$$

Finally, inserting equation (15) into equation (4) yields

$$\sigma^2_{\rho/\rho_0}=\int_1^{\rho/\rho_0}\left(1-\frac{\rho_0}{\rho_2}\right)^2\mathrm{d}\left(\frac{\rho_2}{\rho_0}\right)=\frac{\rho}{\rho_0}-\frac{\rho_0}{\rho}-2\ln\left(\frac{\rho}{\rho_0}\right). \tag{16}$$

It is important to note that in this formulation, equation (16) is physically meaningless if the lower limit of the integral is set in the range $0<\rho/\rho_0<1$. It is due to the definition adopted for the shock width (equation 14), where the shock thickness is defined only for $\rho_2/\rho_0>1$. For highly supersonic turbulence, which is the regime that concerns us, the assumption $\rho\gg\rho_0$ is valid. Then, the first term in equation (16) dominates the variance and we get

$$\sigma^2_{\rho/\rho_0}\approx\frac{\rho}{\rho_0}. \tag{17}$$

For practical reasons, we prefer to consider the variance of the logarithm of the density contrast, $s=\ln(\rho/\rho_0)$, instead of the variance of the linear density when we will compare this analytical model with numerical simulations. These variances are related by (e.g. Federrath et al. 2008b; Price et al. 2011)

$$\sigma_s^2=\ln\left[1+\sigma^2_{\rho/\rho_0}\right]. \tag{18}$$

We now insert the three cases considered in Section 2.1 into equation (18), in order to obtain the density variance–Mach number relation. The subscripts of the following results are chosen based on the value $\alpha=0$, 1/2 and 1 of the $B\propto\rho^\alpha$ relationship.

(i) B independent of ρ: the density variance in this case is exactly the same as for the purely hydrodynamical, isothermal case,

$$\sigma^2_{s,0}=\ln\left[1+b^2\mathscr{M}^2\right]. \tag{19}$$

(ii) $B\propto\rho^{1/2}$: in this case, the density variance is

$$\sigma^2_{s,1/2}=\ln\left[1+b^2\mathscr{M}^2\left(\frac{\beta_0}{\beta_0+1}\right)\right]. \tag{20}$$

This relation is similar to equation (19) except for a correction factor due to the effects of magnetic fields, which is a function of the plasma β_0 only.

(iii) $B\propto\rho$: finally, the density variance–Mach number relation in this case is given by

$$\sigma^2_{s,1}=\ln\left[1+\frac{1}{2}\left(-1-\beta_0+\sqrt{(1+\beta_0)^2+4b^2\mathscr{M}^2\beta_0}\right)\right]. \tag{21}$$

The density variance has a strong dependence on β_0, leaving the rms Mach number as a marginal quantity in this relation.

In the last two cases, when $\beta_0\to0$, the Alfvénic velocity is much higher than the sound speed, and both relations approach zero. In this scenario, the magnetic pressure is infinitely large and prevents density fluctuations from forming. The gas is 'frozen' in the

magnetic field. In the opposite limit, when $\beta_0 \to \infty$, equations (20) and (21) simplify to the purely hydrodynamical case, as expected. In the next section, we are going to test these cases with numerical simulations.

3 NUMERICAL TEST OF THE ANALYTICAL MODEL

3.1 Simulations

We have performed simulations of the evolution of the turbulent, dense, inviscid, magnetized (MHD) and unmagnetized [hydrodynamic (HD)], isothermal interstellar medium using a modified version of the ZEUS-MP hydrodynamical code (Norman 2000; Hayes et al. 2006). We neglect chemical reactions in order to study the effects of magnetic fields in molecular clouds, leaving the inclusion of the effects of chemistry (Glover et al. 2010) for a future study.

Each of our simulations begins with an initially uniform gas distribution, with a mean hydrogen number density of $n_0 = 1000\,\mathrm{cm}^{-3}$ and a resolution of 256^3 cells. The initial velocity field is turbulent, with power concentrated on large scales, between wave numbers $k = 1$ and 2 and with an initial rms velocity of $5\,\mathrm{km\,s}^{-1}$. Moreover, we drive the turbulence so as to maintain approximately the same rms velocity throughout the simulations, following the method described in Mac Low et al. (1998) and Mac Low (1999). We do not perform a Helmholtz decomposition of the force field, and thus the turbulent forcing consists of a natural mixture of solenoidal and compressive modes, i.e. $F_{\rm sol}/(F_{\rm sol} + F_{\rm comp}) \approx 2/3$. Note that Federrath et al. (2008b, 2010) tested the two limiting cases of purely solenoidal (divergence-free) and purely compressive (curl-free) forcing, as well as various mixtures of solenoidal and compressive modes of the turbulent forcing. They found a strong influence on the density PDF, producing a three times larger standard deviation for compressive forcing compared to solenoidal forcing. They parametrized the influence of the forcing by introducing the b-parameter in equation (3). Purely solenoidal forcing is characterized by $b = 1/3$, while purely compressive forcing gives $b = 1$. For the natural mixture, they find $b \approx 0.4$. Using the present set of numerical models, we confirm that using $b = 0.4$ for the natural mixture of forcing modes used here gives the best fits with our analytically derived density variance–Mach number relation. The temperature of the gas is constant and fixed to an initial value $T_0 = 1062$, 170, 42 and 15 K, in order to sample a large set of Mach numbers $\langle\mathscr{M}\rangle \simeq 2, 5, 10$ and 17, respectively. We adopt periodic boundary conditions for the gas using a cubical simulation volume with a side length $L = 20$ pc, such that the turbulent crossing time, $T_{\rm cross} = L/(2c_{\rm s}\mathscr{M}) \approx 2$ Myr. We present results from $t = 3\,T_{\rm cross} \approx 5.7$ Myr, sampled every $0.17\,T_{\rm cross}$, and evolved until $t = 4\,T_{\rm cross} \approx 7.6$ Myr. This period of time is long enough to expect the turbulence to have reached a statistical steady state (Federrath, Klessen & Schmidt 2009; Federrath et al. 2010; Glover et al. 2010; Price & Federrath 2010). This simulation time might be also short enough to obtain reliable results for the initial phase of star formation, when self-gravity did not yet have a large effect on the dynamics. In order to concentrate on turbulent compression alone, we neglect self-gravity in the present experiments.

For the MHD cases, the simulations begin with a uniform magnetic field that is initially oriented parallel to the z-axis of the simulation. Four of these simulations begin with an initial magnetic field strength $B_{\rm i} = 5.85\,\mu$G, which is our standard magnetic field strength hereafter. We also perform three MHD runs with $B_{\rm i} = 10$, 20 and 60 μG, with $\mathscr{M} = 10$, to check the behaviour of the results with increasing magnetic field strengths. We note that as the simulations run, dynamo amplification can lead to increased field strength, and thus we use the instantaneous magnetic field strength to compute β_0. Nevertheless, for simplicity we use the initial value of the magnetic field strength to label runs MHD-B2, MHD-B20 and MHD-B60.

Table 1. List of simulations.

	$B_{\rm i}$	$\langle\beta_0\rangle \pm 1\sigma$	$\langle\mathscr{M}_{\rm A,0}\rangle \pm 1\sigma$	$\langle\sigma_s\rangle \pm 1\sigma$	$\langle\mathscr{M}\rangle \pm 1\sigma$
HD-M2	0	∞	0	0.77 ± 0.02	2.21 ± 0.02
HD-M5	0	∞	0	1.3 ± 0.1	5.4 ± 0.1
HD-M10	0	∞	0	1.7 ± 0.1	10.6 ± 0.2
HD-M17	0	∞	0	1.92 ± 0.09	17.6 ± 0.5
MHD-M2	5.85	25 ± 5	8.1 ± 0.9	0.69 ± 0.02	2.09 ± 0.02
MHD-M5	5.85	4.8 ± 0.4	8.4 ± 0.8	1.18 ± 0.04	4.98 ± 0.07
MHD-M10	5.85	1.4 ± 0.5	9 ± 3	1.47 ± 0.06	10.2 ± 0.3
MHD-M17	5.85	0.3 ± 0.1	7 ± 2	1.61 ± 0.06	16.8 ± 0.5
MHD-B2	2	11.3 ± 0.5	27 ± 2	1.58 ± 0.09	10.5 ± 0.2
MHD-B20	20	0.083 ± 0.005	1.94 ± 0.06	1.48 ± 0.01	9.9 ± 0.2
MHD-B60	60	0.030 ± 0.001	1.24 ± 0.03	1.34 ± 0.01	10.3 ± 0.1

$B_{\rm i}$ – initial magnetic field strength in μG.
β_0 – mean thermal to instantaneous magnetic pressure ratio.
$\mathscr{M}_{\rm A,0}$ – rms Alfvénic Mach number.
σ_s – density variance.
$\mathscr{M}$ – rms Mach number.
The brackets indicate the time average calculated over the snapshots after averaging over the spatial coordinates.

In Table 1, we list the simulations that we have performed. In our labels, we use 'H' to denote a HD run and 'MHD' to denote a MHD run. Our multiple runs with fixed (or zero) magnetic field strength but different sound speeds are labelled with an 'M', followed by the (approximate) rms Mach number of the simulation. Finally, the three runs in which we examined the effect of varying the initial magnetic field strength are labelled with a 'B', followed by the initial field strength in μG. In Table 1, we also list the values of the quantities: β_0, the rms Alfvénic Mach number $\mathscr{M}_{\rm A,0} = v_0/v_{\rm A,0}$ and the sonic Mach number. They are measured in every cell and then are spatially averaged over the data cube. The brackets denote the time average over the seven snapshots, and 1σ shows the temporal standard deviation around the mean values.

3.2 Statistical analysis

In this subsection, we explain the method used to measure the density variance for every snapshot in our simulations using the PDF as a robust statistical tool for this analysis (Price et al. 2011). Then, we parametrize the instantaneous β_0 in terms of $\mathscr{M}$, in the direction of testing numerically the σ_s–$\mathscr{M}$ relations presented in Section 2.2. Finally, we present the comparison between our analytical model and the simulations.

3.2.1 Probability density function (PDF)

In Fig. 1, we plot the volume-weighted dimensionless density PDFs for MHD and HD isothermal gas with the same Mach number for comparison. For these simulations, we find that all the PDFs have a lognormal shape around their peak. However, the PDFs deviate from lognormality especially in the HD simulations at low densities, being more evident for $\mathscr{M} \gtrsim 5$. The error bars in this figure show the 1σ variations around the time average. We see that these variations cannot explain the tail at low densities. Therefore, this deviation

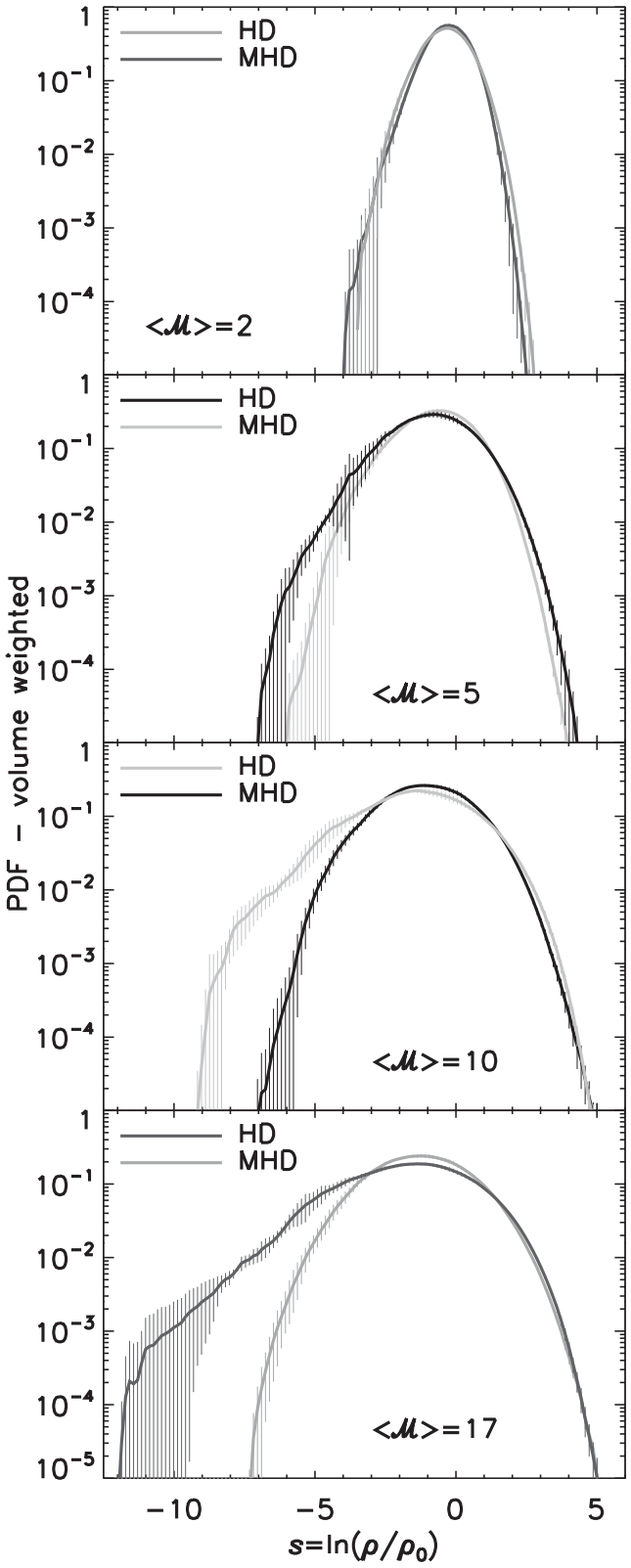

Figure 1. Dimensionless density PDF for magnetized and unmagnetized molecular clouds with the same initial conditions, $n_0 = 1000\,\mathrm{cm}^{-3}$, and the same turbulent rms velocity, but different sound speed. The most significant features are (1) the density variance increases with Mach number and (2) the density variance decreases with magnetic field strength. These simulations have a ratio between thermal pressure and magnetic pressure $\beta_0 \lesssim 10$. All simulations have a resolution of 256^3 zones.

is not explained by intermittency fluctuations, and deserves further study. However, the low-density tail does not significantly affect our σ_s estimates, because the variance is computed from a lognormal fit in a limited interval around the peak, giving the most reliable estimates of σ_s (see Price et al. 2011). In this sense, the trend of the time averages observed between MHD and HD simulations shows the magnetic field acting as a density cushion, preventing the gas from reaching very low densities during local expansion. As a consequence, there are larger parts of the volume with density $\rho \approx \rho_0$ in the MHD case than in the HD case.

In order to avoid contamination from intermittency, numerical artefacts, etc., in the wings of the PDFs, we perform a Gaussian fitting only in a data subset selected by s, in each simulation. This subset consists of 60 per cent of the number of bins considered to calculate the density PDF which are distributed symmetrically around the mean, s_0. Then, we fit the Gaussian profile given by equation (2) to obtain σ_s in every snapshot of the simulations.

3.2.2 *Density variance–rms Mach number test*

In the interest of comparing the density variance–Mach number relation, given by equations (20) and (21), with the results obtained in the previous subsection, we parametrize the thermal-to-magnetic pressure ratio in terms of the rms Mach number for our sequence of simulations. In this sense, we rewrite equation (7) as

$$\beta_0 = 2\frac{\mathcal{M}_{\mathrm{A},0}^2}{\mathcal{M}^2}. \tag{22}$$

Note that this parameter is calculated considering the instantaneous magnetic field strength and not the initial value.

Next, we select the four MHD simulations with different rms Mach number, but the same initial magnetic field strength, and use a linear regression considering the logarithm of equation (22): $\log_{10}\beta_0 = \log_{10} C - 2\log_{10}\mathcal{M}$. From the fit shown in Fig. 2, we find $C = 111 \pm 4$. In Fig. 2, we plot β_0 as a function of the rms Mach number for the different snapshots. The triangles show β_0 for the selected simulations with $\langle\mathcal{M}\rangle \approx 2$, 5, 10 and 17, while the curve shows the linear regression.

In Fig. 3, we combine the dimensionless standard deviation σ_s, obtained from the fit over the numerical PDFs for every snapshot, and the analytical prediction for the three cases of $B \propto \rho^{\alpha}$

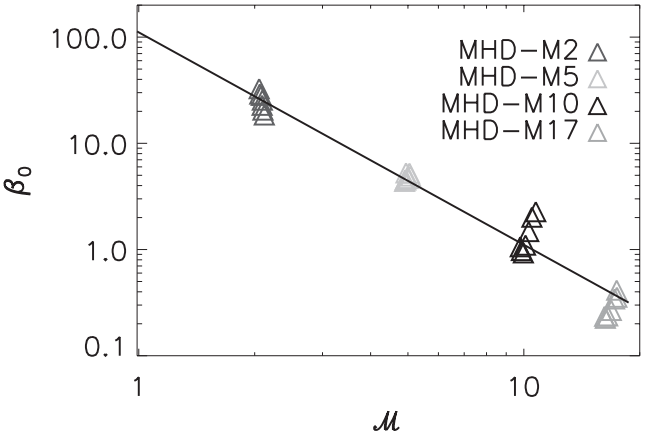

Figure 2. Parametrization of $\beta_0 = P_{\mathrm{th}}/P_{0,\mathrm{mag}}$ with respect to the rms Mach number for the subset of simulations with roughly constant Alfvénic Mach number, $\mathcal{M}_{\mathrm{A},0} \approx 8$ (see Table 1). The curve is a linear regression of the MHD simulations with $B_{\mathrm{i}} = 5.85\,\mu\mathrm{G}$. The linear regression performed to the logarithm of equation (22) gives $\beta_0 = (111 \pm 4).\mathcal{M}^{-2}$.

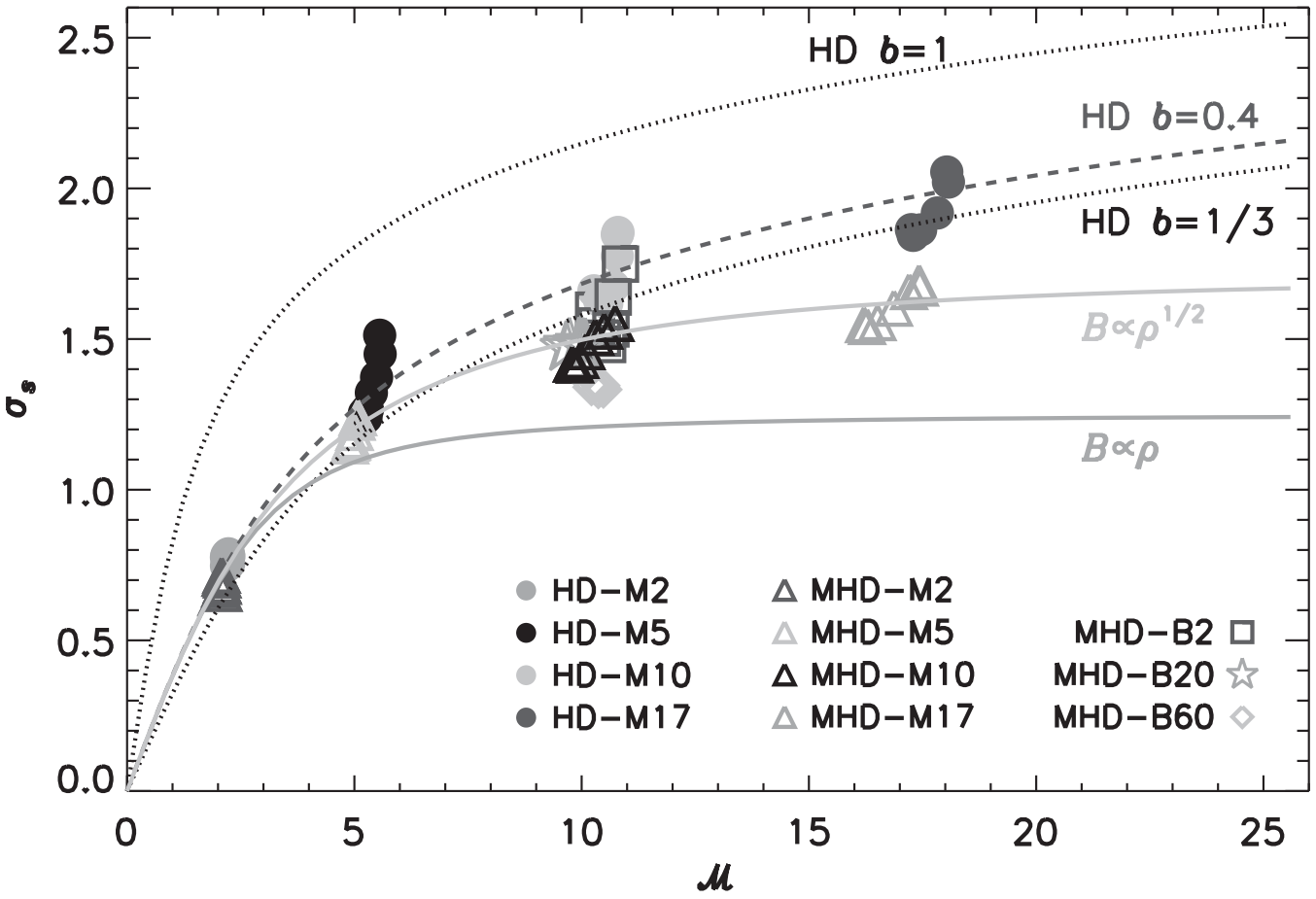

Figure 3. Standard deviation of the dimensionless density contrast, plotted as a function of the rms Mach number. Circles show the purely hydrodynamical simulations that follow very well the Padoan et al. (1997) prediction, $\sigma^2_{s,\rm HD} = \ln(1 + b^2\mathscr{M}^2)$, with $b = 0.4$, expected for mixed-mode turbulent forcing (dashed line; Federrath et al. 2010). The dotted lines are for comparison with purely hydrodynamical model, assuming $b = 1/3$ for purely solenoidal forcing and $b = 1$ for purely compressive forcing (Federrath et al. 2008b). Triangles show the MHD simulations and the two formulae, equations (20) and (21), obtained in this work: $\sigma_{s,1/2} = \{\ln[1 + b^2\mathscr{M}^2\beta_0/(\beta_0 + 1)]\}^{1/2}$ (light grey solid line) and $\sigma_{s,1}$ (dark grey solid line). Those curves are plotted for $b = 0.4$, and using our parametrization, $\beta_0 = (111 \pm 4)\mathscr{M}^{-2}$ from Fig. 2. Squares, stars and diamonds show the additional MHD simulations with different rms Alfvénic Mach number, $\mathscr{M}_{\rm A,0} \approx 27$ ($B_{\rm i} = 2$ μG), $\mathscr{M}_{\rm A,0} \approx 1.9$ ($B_{\rm i} = 20$ μG) and $\mathscr{M}_{\rm A,0} \approx 1.2$ ($B_{\rm i} = 60$ μG).

– with α =0, 1/2 and 1 – as a function of the rms Mach number. For the triangles around a given $\langle\mathscr{M}\rangle$, the HD simulations exhibit larger σ_s compared to the MHD simulations, as was expected from Fig. 1. For comparison, we plot the analytical prediction given by equation (19), $\sigma_{\alpha,0}$. This result matches the prediction provided by Padoan et al. (1997). However, instead of using their proportionality parameter $b \approx 0.5$, we used the input value $b = 0.4$ (dashed line; Federrath et al. 2010), which is the result of the natural mixing of solenoidal and compressive modes in the turbulent forcing field. We also plot the two extreme cases for the unmagnetized gas, $\sigma_{s,\rm HD}$, with $b = 1/3$ (lower dotted line) for purely solenoidal forcing and $b = 1$ for purely compressive forcing (upper dotted line) for comparison.

In the same figure, we superpose equation (20) (light grey solid line) and equation (21) (dark grey solid line), both again with $b = 0.4$. We find that the best agreement with the MHD simulations is given by equation (20), i.e. $\sigma_{s,1/2}$. The result obtained for the first case – B independent of density (equation 19) – may account only for low Mach number zones. This case might be appropriate for diffuse clouds (Crutcher et al. 2010), where the mean sound speed of the cloud may be of the same order as the rms velocity. Here, at $\mathscr{M} \sim 1$, all the three cases converge to the HD result.

Our results are qualitatively in agreement with Ostriker et al. (2001) and Price et al. (2011). These authors find that the density variance in magnetized gas is significantly lower than in the HD counterparts for simulations with a Mach number $\mathscr{M} \gtrsim 10$. In addition, Cho & Lazarian (2003) study the density contrast resulting from the Alfvénic waves, slow and fast magnetosonic waves originating in different environments. The authors concluded that the three kinds of waves can coexist in those environments. In the regime that concerns us, $\beta_0 \approx 1$ and $5 \lesssim \mathscr{M} \lesssim 10$, their density contrasts closely match ours.

To test the validity of our results for different Alfvénic Mach numbers, we also performed three simulations with an initial magnetic field strength different from the standard one, with $\mathscr{M}_{\rm A,0} \approx 27$, 1.9 and 1.2, at $\langle\mathscr{M}\rangle \approx 10$ (empty squares in Fig. 3). Our model works well for $\mathscr{M}_{\rm A,0} \gtrsim 6$, but breaks down for our test with $\mathscr{M}_{\rm A,0} \lesssim 2$. The break occurs when the turbulence becomes trans-Alfvénic or sub-Alfvénic, i.e. when $\mathscr{M}_{\rm A,0} \lesssim 2$. This is due to anisotropies arising in this case, i.e. the turbulence is no longer isotropic, as can be seen in Fig. 4. This is because the back reaction of the magnetic field on to the flow is extremely strong for flows perpendicular to the magnetic field lines, if the turbulence is trans-Alfvénic or sub-Alfvénic (see e.g. Cho & Lazarian 2003; Brunt, Federrath & Price

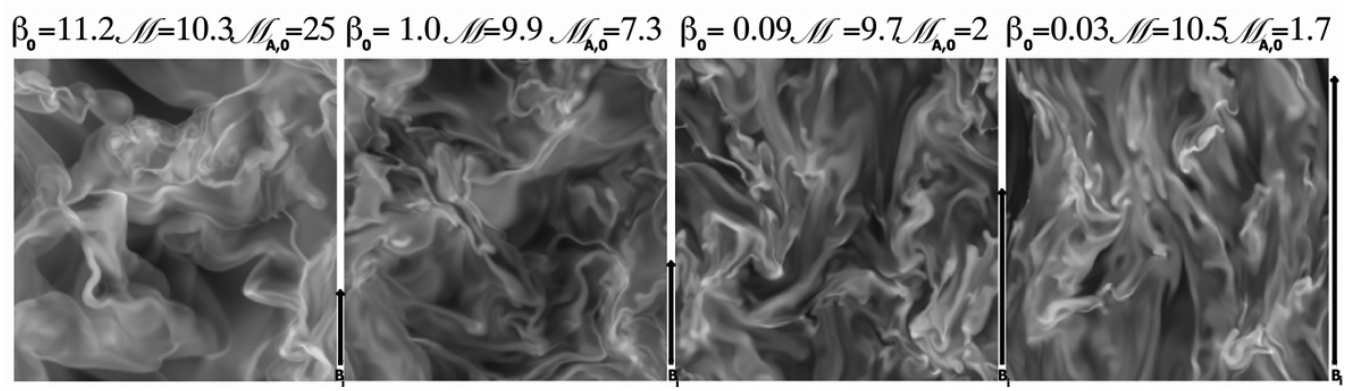

Figure 4. Density slices of the simulations at $t = 6$ Myr. The mean magnetic field is oriented along the vertical axis. From left to right: initial magnetic field strength $B_i = 2$, 5.85, 20 and 60 μG. The turbulence remains isotropic for super-Alfvénic gas $\mathcal{M}_{A,0} \gg 1$, but when it becomes trans-Alfvénic or sub-Alfvénic ($\mathcal{M}_{A,0} \lesssim 3$), the turbulence becomes highly anisotropic.

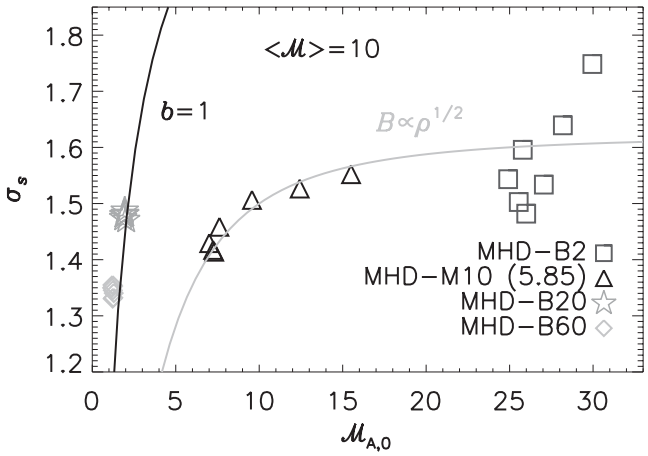

Figure 5. Standard deviation of the dimensionless density contrast, plotted as a function of the instantaneous rms Alfvénic Mach number at $\langle\mathcal{M}\rangle \approx 10$. The different symbols show snapshots of simulations with $\mathcal{M}_{A,0}$ time averages: $\langle\mathcal{M}_{A,0}\rangle \approx 27$ (squares), $\langle\mathcal{M}_{A,0}\rangle \approx 9$ (triangles), $\langle\mathcal{M}_{A,0}\rangle \approx 1.9$ (stars) and $\langle\mathcal{M}_{A,0}\rangle \approx 1.2$ (diamonds). When the turbulence becomes trans-Alfvénic or sub-Alfvénic, $\langle\mathcal{M}_{A,0}\rangle \lesssim 2$ (stars and diamonds), anisotropies arise in the gas, because the back reaction of the magnetic field on to the flow is extremely strong for flows perpendicular to the magnetic field lines. The grey curve shows our prediction (see footnote 1) using $b \approx 0.4$ that fits very well the data. Meanwhile, the black curve shows our prediction (see footnote 1) considering $b = 1$ (corresponding to purely compressive forcing). Although our turbulent forcing in the simulations is by definition mixed, and thus we expect $b \approx 0.4$ (Federrath et al. 2010), it is noteworthy to say that $b = 1$ gives a good fit to the data with very low $\langle\mathcal{M}_{A,0}\rangle \lesssim 2$.

2010; Esquivel & Lazarian 2011). Since our analytic derivation is based on an ensemble average (equation 4), assuming statistical isotropy, the anisotropies are the most likely cause for the limitation of our model to super-Alfvénic turbulence. In Fig. 5, we show our prediction (equation 20)[1] for a fixed Mach number $\mathcal{M} \approx 10$ and forcing parameter $b \approx 0.4$, which fits very well the data with $\mathcal{M}_{A,0} \gtrsim 6$. These simulations show high dispersion – around the time average – in the density variance and the rms Alfvénic Mach number showing the fluctuations of the gas caused by the turbulence dominating the dynamics of the flow, in contraposition of the simulations with small Alfvénic Mach number. In the same figure, we also plot the model curve equation (20) for the same sonic Mach number 10 and $b = 1$. Although our turbulent forcing in the simulations is by definition mixed, and thus we expect $b \approx 0.4$ (Federrath et al. 2010), we find it interesting to note that $b = 1$ – corresponding to purely compressive forcing – gives a good fit to the data with very low Alfvénic Mach number, $\mathcal{M}_{A,0} \lesssim 2$. We speculate that the density field for very high magnetic field strengths and thus very low Alfvénic Mach number starts behaving as if it was driven by purely compressive forcing. This is very different from the compression obtained with solenoidal or mixed forcing, but more similar to compressive forcing, which also directly compresses the gas (Federrath et al. 2008b). More data at $\mathcal{M}_{A,0} \lesssim 2$ would be needed to sample this region and the transition from $b = 0.4$ to 1 in detail, and we just note here that $b = 1$ seems to provide a good fit for $\mathcal{M}_{A,0} \lesssim 2$, given the data at hand.

[1] Equation (20) has been written in terms of the instantaneous Alfvénic Mach number (equation 22), yielding the relation for the density variance: $\sigma^2_{s,1/2} = \ln[1 + 2b^2\mathcal{M}^2\mathcal{M}^2_{A,0}/(2.\mathcal{M}^2_{A,0} + \mathcal{M}^2)]$.

4 CONCLUSIONS

We presented an analytical prediction for the density variance–Mach number relation in magnetized supersonic turbulent gas. In this formulation, we considered three different cases for the relation between the magnetic field strength and density. The first case assumes that B is independent of ρ, the second assumes that $B \propto \rho^{1/2}$, while the third is given by $B \propto \rho$. The three resulting σ_s–$\mathcal{M}$ relations were tested against numerical simulations. From this analysis we conclude that the following.

(i) If B is independent of the density, we recover the hydrodynamical prediction of Padoan et al. (1997). In this case, the gas and the magnetic field are not coupled. Therefore, an amplification of the magnetic field with the shock is not expected. Observationally, Crutcher (1999) found that the magnetic field was independent of the density for diffuse clouds, corresponding to low rms Mach numbers, $\mathcal{M} \lesssim 2$. In this regime, all our predictions converge to the purely hydrodynamical σ_s–$\mathcal{M}$ relation.

(ii) For the second case, $B \propto \rho^{1/2}$, we found a one-to-one relation between $\mathcal{M}$, β_0 and the density variance. This σ_s–$\mathcal{M}$ relation (equation 20) matches very well our numerical test considering $b = 0.4$, which is the input for the natural mixture of compressive-to-solenoidal modes in the turbulent forcing field. This result is in agreement with the ones presented by Ostriker et al. (2001) and Price et al. (2011), where they found lower σ_s than in

the unmagnetized case for $\mathscr{M} \gtrsim 10$. Moreover, Cho & Lazarian (2003) presented a density contrast that closely matches our result for $\beta_0 \approx 1$ and $5 \lesssim \mathscr{M} \lesssim 10$.

(iii) For the last case, $B \propto \rho$, the σ_s–$\mathscr{M}$ relation (equation 21) predicts a lower density variance than measured in our numerical simulations for $\mathscr{M} \geq 5$, because our simulations are closer to $B \propto \rho^{1/2}$. However, the relation given by equation (21) would fit better, if $B \propto \rho$.

(iv) The σ_s–$\mathscr{M}$ relation obtained for $B \propto \rho^{1/2}$ works very well for intermediate to high Alfvénic Mach number, $\mathscr{M}_{\rm A,0} \gtrsim 6$, but breaks down for $\mathscr{M}_{\rm A,0} \lesssim 2$ at $\langle \mathscr{M} \rangle \approx 10$. This probably occurs because in the presence of strong magnetic fields, the turbulence is no longer isotropic. This is because the back reaction of the magnetic field on to the flow is very strong for flows perpendicular to the magnetic field lines.

Magnetic fields act as a density cushion in turbulent gas, preventing the gas from reaching very low densities as well as very high densities. We conclude that magnetic fields are an important mechanism for shaping the density variance–Mach number relation, and therefore will change the quantitative predictions in models of the star formation rate, initial mass function or core mass function that depend on these quantities (e.g. Padoan & Nordlund 2002, 2011; Krumholz & McKee 2005; Hennebelle & Chabrier 2008, 2009).

ACKNOWLEDGMENTS

We thank the anonymous referee for the useful comments that helped improve this manuscript. FZM thanks Paola Pinilla and Joe Ramsey for reading the manuscript and providing useful comments, as well as the International Max Planck Research School for Astronomy and Cosmic Physics at the University of Heidelberg, and the Heidelberg Graduate School of Fundamental Physics. FZM received funding from the German Bundesministerium für Bildung und Forschung for funding via the ASTRONET project STAR FORMAT (grant 05A09VHA) CF received funding from a Discovery Projects fellowship by the Australian Research Council (grant DP110102191) and from the European Research Council (FP7/2007-2013 grant agreement no. 247060). All authors acknowledge subsidies from the Baden-Württemberg-Stiftung for contract research via grant P-LS-SPII/18 and the Deutsche Forschungsgemeinschaft via SFB project 881 'The Milky Way System' (subprojects B1, B2, B3 and B5) as well as the SPP 1573 'The Physics of the ISM'. The simulations described in this paper were performed using the Ranger cluster at the Texas Advanced Computing Center, using time allocated as part of Teragrid project TG-MCA99S024.

REFERENCES

Banerjee R., Vázquez-Semadeni E., Hennebelle P., Klessen R. S., 2009, MNRAS, 398, 1082
Bertram E., Federrath C., Banerjee R., Klessen R. S., 2012, MNRAS, 420, 3163
Brunt C. M., Heyer M. H., Mac Low M.-M., 2009, A&A, 504, 883
Brunt C. M., Federrath C., Price D. J., 2010, MNRAS, 403, 1507
Cho W., Kim J., 2011, MNRAS, 410, L8
Cho J., Lazarian A., 2003, MNRAS, 345, 325
Collins D. C., Padoan P., Norman M. L., Xu H., 2011, ApJ, 731, 59
Crutcher R. M., 1999, ApJ, 520, 706
Crutcher R., Heiles C., Troland T., 2003, in Falgarone E., Passot T., eds, Lect. Notes Phys. Vol. 614, Turbulence and Magnetic Fields in Astrophysics. Springer-Verlag, Berlin, p. 155
Crutcher R. M., Hakobian N., Troland T. H., 2009, ApJ, 692, 844
Crutcher R. M., Wandelt B., Heiles C., Falgarone E., Troland T. H., 2010, ApJ, 725, 466
Dyson J. E., Williams D. A., 1980, in Dyson J. E., Williams D. A., eds, Physics of the Interstellar Medium. Halsted Press, New York, p. 204
Elmegreen B. G., Scalo J., 2004, ARA&A, 42, 211
Esquivel A., Lazarian A., 2011, ApJ, 740, 117
Federrath C., Glover S. C. O., Klessen R. S., Schmidt W., 2008a, Phys. Scr. Vol. T, 132, 014025
Federrath C., Klessen R. S., Schmidt W., 2008b, ApJ, 688, L79
Federrath C., Klessen R. S., Schmidt W., 2009, ApJ, 692, 364
Federrath C., Roman-Duval J., Klessen R. S., Schmidt W., Mac Low M.-M., 2010, A&A, 512, A81
Federrath C., Sur S., Schleicher D. R. G., Banerjee R., Klessen R. S., 2011, ApJ, 731, 62
Fleck R. C., Jr, 1982, MNRAS, 201, 551
Glover S. C. O., Mac Low M.-M., 2007, ApJ, 659, 1317
Glover S. C. O., Federrath C., Mac Low M.-M., Klessen R. S., 2010, MNRAS, 404, 2
Hayes J. C., Norman M. L., Fiedler R. A., Bordner J. O., Li P. S., Clark S. E., ud-Doula A., Mac Low M.-M., 2006, ApJS, 165, 188
Hennebelle P., Chabrier G., 2008, ApJ, 684, 395
Hennebelle P., Chabrier G., 2009, ApJ, 702, 1428
Hennebelle P., Pérault M., 2000, A&A, 359, 1124
Kainulainen J., Beuther H., Henning T., Plume R., 2009, A&A, 508, L35
Kim J., Balsara D., Mac Low M.-M., 2001, J. Korean Astron. Soc., 34, 333
Klessen R. S., 2000, ApJ, 535, 869
Klessen R. S., Burkert A., 2000, ApJS, 128, 287
Kritsuk A. G., Norman M. L., Padoan P., Wagner R., 2007, ApJ, 665, 416
Kritsuk A. G., Norman M. L., Wagner R., 2011, ApJ, 727, L20
Krumholz M. R., McKee C. F., 2005, ApJ, 630, 250
Landau L. D., Lifshitz E. M., 1987, in Landau L. D., Lifshitz E. M., eds, Fluid Mechanics. Pergamon Press, Oxford, p. 459
Lemaster M. N., Stone J. M., 2008, ApJ, 682, L97
Lequeux J., 2005, The Interstellar Medium. Springer-Verlag, Berlin, p. 244
Li Y., Klessen R. S., Mac Low M.-M., 2003, ApJ, 592, 975
Li P. S., Norman M. L., Mac Low M.-M., Heitsch F., 2004, ApJ, 605, 800
McKee C. F., Ostriker E. C., 2007, ARA&A, 45, 565
Mac Low M.-M., 1999, ApJ, 524, 169
Mac Low M.-M., Klessen R. S., 2004, Rev. Modern Phys., 76, 125
Mac Low M.-M., Klessen R. S., Burkert A., Smith M. D., 1998, Phys. Rev. Lett., 80, 2754
Mouschovias T. C., Ciolek G. E., 1999, in Lada C. J., Kylafis N. D., eds, Proc. NATO ASIC Vol. 540, The Origin of Stars and Planetary Systems. Kluwer, Dordrecht, p. 305
Nordlund Å. K., Padoan P., 1999, in Franco J., Carraminana A., eds, Proc. 2nd Guillermo Haro Conference, Interstellar Turbulence. Cambridge Univ. Press, Cambridge, p. 218
Norman M. L., 2000, Rev. Mex. Astron. Astrofis. Ser. Conf. 9, 66
Ossenkopf V., Mac Low M.-M., 2002, A&A, 390, 307
Ostriker E. C., Stone J. M., Gammie C. F., 2001, ApJ, 546, 980
Padoan P., Nordlund Å., 1999, ApJ, 526, 279
Padoan P., Nordlund Å., 2002, ApJ, 576, 870
Padoan P., Nordlund Å., 2011, ApJ, 730, 40
Padoan P., Nordlund A., Jones B. J. T., 1997, MNRAS, 288, 145
Passot T., Vázquez-Semadeni E., 1998, Phys. Rev. E, 58, 4501
Pope S. B., Ching E. S. C., 1993, Phys. Fluids A, 5, 1529
Press W. H., Schechter P., 1974, ApJ, 187, 425
Price D. J., Federrath C., 2010, MNRAS, 406, 1659
Price D. J., Federrath C., Brunt C. M., 2011, ApJ, 727, L21
Scalo J., Vazquez-Semadeni E., Chappell D., Passot T., 1998, ApJ, 504, 835

Schleicher D. R. G., Banerjee R., Sur S., Arshakian T. G., Klessen R. S., Beck R., Spaans M., 2010, A&A, 522, A115
Schmidt W., Federrath C., Hupp M., Kern S., Niemeyer J. C., 2009, A&A, 494, 127
Sur S., Schleicher D. R. G., Banerjee R., Federrath C., Klessen R. S., 2010, ApJ, 721, L134
Vázquez-Semadeni E., 1994, ApJ, 423, 681
Wada K., 2001, ApJ, 559, L41
Zinnecker H., 1984, MNRAS, 210, 43

This paper has been typeset from a TEX/LATEX file prepared by the author.